

RSC Advances



This is an *Accepted Manuscript*, which has been through the Royal Society of Chemistry peer review process and has been accepted for publication.

Accepted Manuscripts are published online shortly after acceptance, before technical editing, formatting and proof reading. Using this free service, authors can make their results available to the community, in citable form, before we publish the edited article. This *Accepted Manuscript* will be replaced by the edited, formatted and paginated article as soon as this is available.

You can find more information about *Accepted Manuscripts* in the [Information for Authors](#).

Please note that technical editing may introduce minor changes to the text and/or graphics, which may alter content. The journal's standard [Terms & Conditions](#) and the [Ethical guidelines](#) still apply. In no event shall the Royal Society of Chemistry be held responsible for any errors or omissions in this *Accepted Manuscript* or any consequences arising from the use of any information it contains.

Cite this: DOI: 10.1039/c0xx00000x

www.rsc.org/xxxxxx

ARTICLE TYPE

Preparation of Macroporous Flexible Three Dimensional Graphene Sponge Using Ice-Template as Anode Material for Microbial Fuel Cell

Wufeng Chen^{a‡}, Yu-Xi Huang^{b‡}, Dao-Bo Li^b, Han-Qing Yu^b, Lifeng Yan^{a*}*Received (in XXX, XXX) Xth XXXXXXXXX 20XX, Accepted Xth XXXXXXXXX 20XX*

DOI: 10.1039/b000000x

A simple and effective method for the fabrication of flexible macroporous 3D graphene sponge using ice template is developed in this work. It was found that the porous structures of the 3D graphene architecture depended on the rate of ice crystal formation. At a low cooling rate, the inner walls of the graphene hydrogel were re-assembled into hierarchical macroporous structure by the as-formed ice crystals, resulting in the formation of macroporous graphene sponge after freeze-drying. The as-prepared graphene sponge was flexible and could recover from a 50% deformation. As the graphene sponge was used as the anode of a microbial fuel cell (MFC), the maximum power density reached 427.0 W m⁻³, which was higher than that of the MFC fabricated using carbon felt as the anode material. The macroporous structure of the graphene sponge ensured the microbes more easily be diffused and propagated inside the materials, resulting in the higher MFC performance.

Introduction

Microbial fuel cell (MFC) is a bio-electrochemical system that drives a current by using bacteria and mimicking bacterial interactions. Typical MFC is a device that converts chemical energy to electrical energy by the catalytic reaction of microorganisms. ¹ Typically, an MFC consists of anode and cathode compartments separated by a membrane. In the anode compartment, fuel is oxidized by microorganisms, generating CO₂, electrons and protons. Electrons are transferred to the cathode compartment through an external electric circuit, while protons are transferred to the cathode compartment through the membrane. Recently MFCs have attracted great interests as they are recognized as the next generation of green energy. ^{1,2}

Generally, different types of carbon-based materials, such as carbon foam,³ carbon mesh⁴ and carbon felt,⁵ are used as electrode materials for MFCs. So far the studies of these materials focus on two aspects: large surface area and porous structure, which allow the maximized colonization and strong interaction, high conductivity and good biocompatibility to facilitate extracellular electron transfer. Graphene, a famous member in carbon family, owns potential properties such as high electrical conductivity,⁶ large specific surface area,⁷ high thermal conductivity⁸ and mechanical strength.⁵ Building upon the nanosheets of graphene, three dimensional (3D) architectures of graphene have attracted tremendous attention for their wide applications including Li-ion batteries,⁹ supercapacitors,^{10,11} sensors¹² and oil sorbents.¹³ Commercial electrodes modified by graphene have been also used in MFCs,¹⁴⁻¹⁶ but little works about the MFC electrode using monolithic 3D graphene have been reported. Graphene sponge-like 3D materials, such as graphene aerogel or foam are weak in elasticity, limiting its application in

flexible electronic devices. Graphene sponge (GS) fabricated by chemical vapor deposition (CVD) method using nickel foam as template showed excellent flexibility,¹⁷ while the fabrication process is of high cost. In our previous work, we found that the nanosheets of graphene oxide could be easily assembled into 3D hydrogel of reduced graphene (rGO) via a chemical reduction induced self-assembly.¹¹ The rGO hydrogel is microporous and it is thus difficult for microbes to enter the inner side of the materials. Is it possible to prepare flexible GS with macroporous structure?

Ice template is a generic method to prepare hierarchical microstructure for polymers or nanoparticles.¹⁸ Thus, it could also be used to tailor the pore structure of graphene aerogel during the freeze-drying process of graphene hydrogel, resulting in flexible graphene sponge. Therefore, in this work we intend to develop a facile and general method to fabricate the flexible 3D GS by ice template. The size and shape of the ice crystal formed during the freezing process depend on the rate of cooling. At a low cooling rate, graphene hydrogel can be assembled into hierarchical macroporous structure by the big ice crystals, resulting in the formation of macroporous structure. Compared with the graphene aerogel prepared by rapid freezing drying, the slow cooling rate favored the formation of big ice crystal and resulted in the formation of flexible 3D GS, which showed a high flexibility and held a great potential as flexible electronics.¹⁹ Thereafter, the as-prepared GS was employed as the anode material in MFCs, and it provided 3D open space with a large area for microbial colonization. Compared with commercial carbon felt as anode, MFC provided performance improved by GS. In addition, this material is also high conductive, light in weight, and of high porosity, which make it a potential materials for practical application.

Experimental

Materials.

Flake graphite, 2-5mm, 99.9% (metals basis) was purchased from Alfa Aesar Co., USA. Analytical grade NaNO_3 , KMnO_4 , 98% H_2SO_4 , 30% H_2O_2 aqueous solution, were purchased from Shanghai Chemical Reagents Co., China, and were used directly without further purification. Ultra-pure water (18 M Ω) was produced by a Millipore System (Millipore Q, USA).

Preparation of GO

GO is prepared from flake graphite by a modified Hummers and Offema method with reoxidation process.²⁰ In brief, 2 g of the flake graphite was added into a 400 mL beaker and 1 g of NaNO_3 and 40 mL of H_2SO_4 were added subsequently under stirring in an ice-bath. Then, 5 g of KMnO_4 was added slowly into the beaker under stirring conditions and the system temperature was kept lower than 20 °C. After that, the reaction system was maintained for 10 h at room temperature. Then, 40 mL of H_2SO_4 and 4 g of KMnO_4 were added, and the reaction was kept for additional 10 h. Thereafter, 100 mL water was slowly added into the system and it was stirred for another 20 min. 80 mL of hot water at 60 °C and 3% H_2O_2 aqueous solution were added to reduce the residual KMnO_4 until the bubbling disappeared. Finally, the suspension was centrifuged at 7200 rpm for 20 min, and the residue was washed by warm water. The obtained sediment was re-dispersed into water and treated by oscillation at frequency of 200 min⁻¹ for 2 days. A homogeneous suspension around 3 mg ml⁻¹ was collected after removing the trace black residues by centrifugation at 3000 rpm for 5 min. GO powders were obtained after freezing and drying of the suspension.

Synthesis of graphene hydrogel and aerogels

Aqueous suspension of GO at concentration of 3 mg ml⁻¹ was prepared as mentioned above, and NaHSO_3 was added as reducing agent. The mixed suspension was heated at 95 °C for 3 h without stirring. The as-prepared hydrogel was dialyzed against deionized water for 3 d. For aerogels preparation, the as-prepared graphene hydrogel was freezing under different cold conditions, and was then freezing-dried to remove water to obtain graphene aerogels.

Operation of MFCs

For MFCs tests, two-bottle configuration MFCs were constructed with half cells separated by a cation exchange membrane (CMI7000, Membranes International Inc., USA). Each bottle had a volume of 120 mL. One piece of rectangular carbon paper (9 cm² for each piece) was used as cathode. Anaerobic sludge was collected from a full-scale upflow anaerobic sludge blanket reactor treating citrate-producing wastewater located in Bengbu, China, and inoculated into the MFCs as the seeding inoculums. The anode chamber was fed with 100 mL of medium containing 0.8 g L⁻¹ of acetate in 50 mM phosphate buffer solution (mixed culture-inoculated MFCs), while the cathode chamber contained 110 mL of 0.1 M $\text{K}_3\text{Fe}(\text{CN})_6$ as the electron receptor. The

experiments were conducted in anaerobic conditions by purging the anode chamber with nitrogen. The output voltage was collected using 34970A Data Acquisition/Switch Unit (Agilent Inc., USA) with an external resistance of 1000 Ω for mixed culture-inoculated MFCs. Polarization curves were obtained by measuring the stable voltage generated at various external resistances and then the maximum power density was evaluated. After each fed-batch cycle, the MFCs were drained, and refilled with substrate solution, and bubbled with nitrogen for 30 min. The mixed culture-inoculated MFCs were operated for four operation cycles, each of which took ~7 d. Generally, three times of MFC experiments were carried out for one condition (one of which usually lasted for 3-4 weeks).

Electrochemical analysis

Electrochemical measurements were conducted with a CHI 660C potentiostat (CH Instruments Inc., Austin, Texas, USA). The electrochemical active surface area of the anode materials was estimated by cyclic voltammetry (CV) using a ferrocyanide solution. The ferrocyanide solution (5 mM, 0.2 M Na_2SO_4 as the supporting electrolyte) was placed in an electrochemical cell, which contained a piece of GS or carbon felt (working electrode, volume 0.8 cm³), a platinum wire (counter electrode) and an Ag/AgCl reference electrode. CV tests were carried out at a scan rate of 50 mV s⁻¹ and over a potential range of 0 to 0.9 V (vs. SHE) (potential was recalculated relative to SHE). Before and after the MFC tests, electrochemical impedance spectroscopy (EIS) was conducted in an electrochemical cell containing 0.1 M KCl with 10 mM $[\text{Fe}(\text{CN})_6]^{3-/4-}$. The EIS parameters were as follows: initial potential was set as an open circuit potential, high frequency = 100000 Hz, low frequency = 0.01 Hz, amplitude = 5 mV.

Characterization of graphene aerogels

The morphologies of the hydrogel and aerogels were characterized by SEM (Sirion 200 SEM, FEI Co., Japan). Elemental analysis was carried out by a VARIO ELIII analyzer (Elemental Co., Germany). The electrical conductivities of samples were measured by two-probe method using a CHI440 potentiostat-galvanostat (CH Instruments Inc., Austin, Texas, USA). TEM images were obtained on a H-800 microscope at 200 kV (Hitachi Co., Japan).

Results and Discussion

Fabrication of graphene sponge using the ice template method

In a previous study we proposed a protocol for 3D graphene architecture preparation *via* a self-assembly during in-situ reduction of graphene oxide, which resulted in the formation of graphene hydrogel.¹⁰ Freeze-drying is a versatile method to prepare graphene aerogel from the hydrogel, and the ice template helps to retain its porous structure. Revisiting this process, it is clear that the porosity of the graphene aerogel can be easily manipulated by the sizes and shapes of the ice crystal, which can be controlled by adjusting the cooling rate.¹⁷

Cite this: DOI: 10.1039/coxx00000x

www.rsc.org/xxxxxx

ARTICLE TYPE

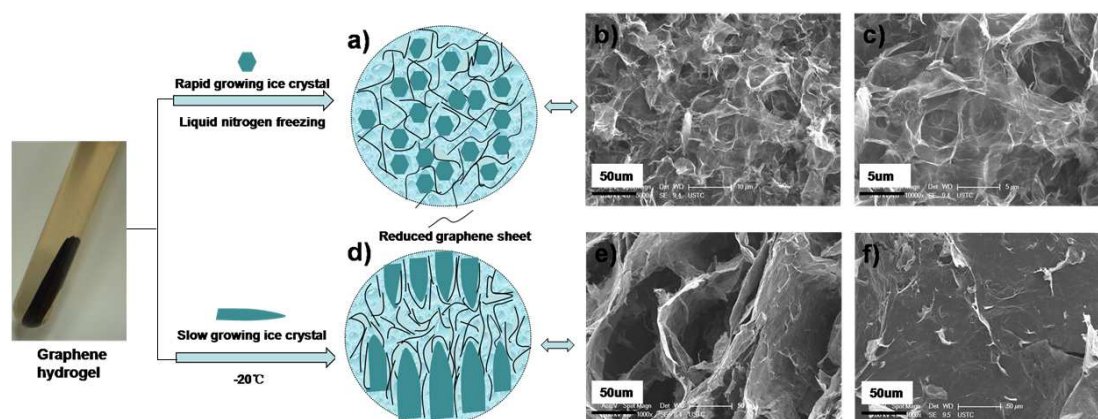


Figure 1. Schematic diagram of the formation process of 3D porous graphene structures induced by ice template at different growing rates of ice crystals (a,d). Cross-sectional SEM images of graphene foam (b,c) and graphene sponge (e) prepared by liquid nitrogen freezing (quick) and -10°C treatment in a refrigerator (slow), respectively. Surface of graphene film of graphene sponge aligned by graphene sheets (f).

Here, the cell walls of the pores in the graphene hydrogel were assembled as the building blocks in the ice template formation process (Figure 1). Two samples were prepared by cooling the hydrogel at -10°C in a refrigerator with a slow growing rate of ice crystal, or by liquid nitrogen cooling for a quick growth of ice crystal, respectively. Liquid nitrogen freezing results in a higher temperature gradient and rapid ice nucleation and growth, and leads to plenty of small ice crystals and isotropic structural ice template (graphene foam, GF). However, when the hydrogel was frozen at -10°C in a refrigerator, the growth of ice crystals prevailed than the ice nucleation, and ice crystals grow along temperature gradient, leading to big and anisotropic ice template. The nanosheets of graphene inside the hydrogel were repelled by ice crystals and stacked into highly ordered film-like structure, with several micrometers in thickness and hundreds of

micrometers (typically 100~500µm according to SEM images) with lateral size. These large graphene films were aligned in near parallel with each other, creating macroporous structure, and the hierarchical structure aerogel was named as graphene sponge (GS). Similar results were reported by Xie et al.¹⁸, who proposed a general protocol to finely tailor the structure of porous graphene by a modified freeze casting process. However, they just reported the method to prepare GS, and the as-prepared materials had not been used in MFC. In addition, a special homemade freezing temperature unit was employed in their study. Here, GS can be easily prepared just by a commercial refrigerator, and the as-prepared GS was used as the anode material for MFC considering its macroporous structure.

Characterization of the graphene aerogels

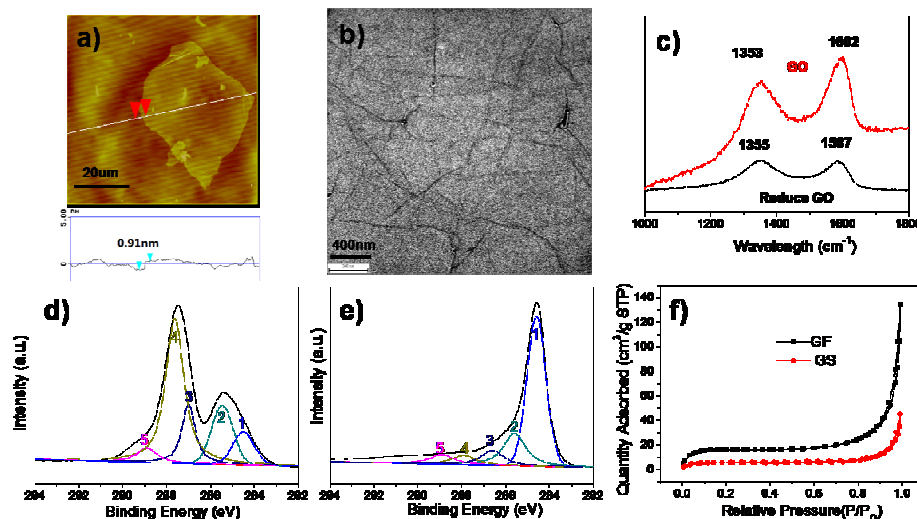


Figure 2. (a) AFM image of single layer large sheet of graphene oxide (GO), (b) TEM image of GO sheet suspended on a Cu grid, (c) Raman spectra of GO and reduced GO, (d,e) XPS profiles of the as-formed GO and reduced GO, and (f) Nitrogen adsorption isotherms of GF and GS.

Cite this: DOI: 10.1039/COXX00000X

www.rsc.org/xxxxxx

ARTICLE TYPE

In addition to the cooling rate, the size of the nanosheets of GO was another important factor to affect the pore structure of the final product. Here, the large sheets (up to 30 μm in lateral size) of GO were employed as the precursor (Fig. 2a). In our previous work, the graphene aerogel was fabricated using GO sheets with lateral size of 2-5 μm by liquid nitrogen freezing, and massive interconnected pores were observed at the cross-section of the aerogel.^{8, 19} For large GO sheets, under the same conditions, the morphology of aerogel was different, and the sheets were overlapped with each other largely, resulting in fewer porous channels. Transmission electron microscopy (TEM) image shows that wrinkle structures appeared on both sides of the sheets (Fig. 2b and Fig. S2), indicating that the large sheets of graphene acted as soft slices, rather than rigid plates. Thus, there were strong connections between the sheets by π - π interaction, enhancing the integrity of graphene monoliths. The Brunauer-Emmett-Teller (BET) specific surface area and porous structure characteristics of the graphene aerogels were examined by nitrogen isothermal adsorption. As shown in Fig. 2f, the BET specific surface area of GS was 55.4 m^2g^{-1} , while for GF the value was 19.9 m^2g^{-1} only due to severe stacking, and both lower than that of graphene aerogel from small GO sheets (117.0 m^2g^{-1}).⁸ The nitrogen adsorption/desorption isotherm study (Fig. 2f) shows that the GF and GS were mesoporous, and their pore size distribution was in

a range of 2-100 nm. BET measurement is merely for small pores, while larger pores up to micrometers could still be observed from the SEM images. The pore volumes of GS and GF determined by Barrett-Joyner-Halenda (BJH) method were 0.197 cm^3g^{-1} and 0.0655 cm^3g^{-1} , respectively.

Raman spectra and XPS were also employed to characterize the large GO and reduced graphene of GS. As shown in Fig. 2c, Raman spectra of GO and GS reveals both D bands and G bands. The peaks at 1353 cm^{-1} and 1355 cm^{-1} corresponded to the D bands of GO and GS, while the peaks at 1602 cm^{-1} and 1587 cm^{-1} were assigned to their G bands respectively. The value I_D/I_G of GS was 0.99, much lower than that of the reduced graphene ($I_D/I_G = 1.22$) from small-sized GO nanosheets,⁶ indicating the efficient reduction of GO sheets in the GS.

The XPS analysis shows the oxygen content decreased from 38.39% to 12.75% from GO to GS, while carbon contents increased from 60.72% to 85.21%. For carbon, comparing the C1s XPS profile in Fig. 2d and 2e, the oxygen species of C-O (hydroxyl and epoxy, 286.9 eV, peak 3), C=O (carbonyl, 287.9 eV, peak 4) of GO were reduced significantly, indicating the efficient deoxidization of GO. The major remaining species of GS were C=C (sp^2 , 284.6 eV, peak 1) and C-C (sp^3 , 285.6 eV, peak 2).

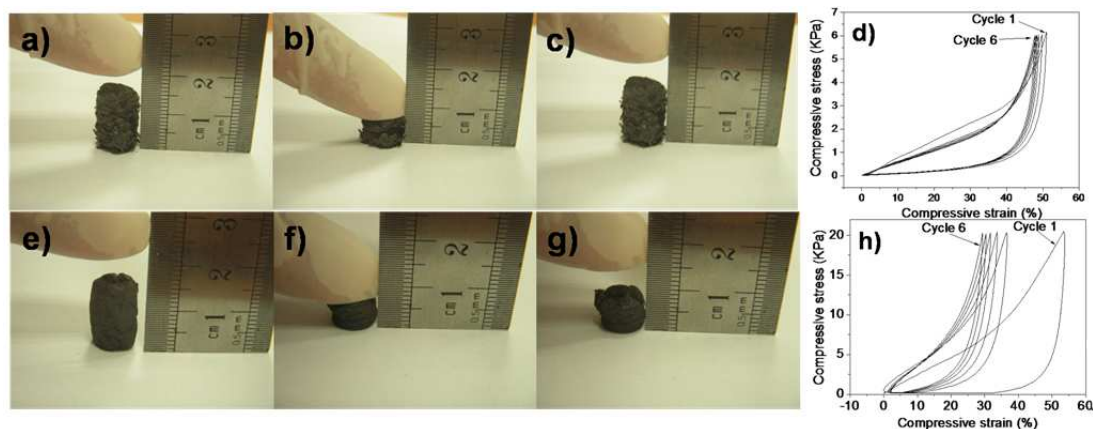


Figure 3. Mechanical properties of GS and GF. Compression-recovery process of GS (a,b,c) and GF (e,f,g) after 50% deformation, and the compressive stress-strain curves of 6 cycles of loading and unloading for GS (d) and GF (h) under respective constant pressure.

Characterization of mechanical properties of the graphene sponges

The microstructures of the GS and GF network ensure their mechanical properties. Compared with GF, the hierarchical GS exhibited an excellent flexibility. As shown in Fig. 3a-c, after the GS was compressed up to 50% strain, it could be recovered well after the force was releasing. However, for GF, it was partially recovered to its original shape only due to the damage of the porous structure, as shown in Fig. 3e-g. In addition, Fig. 3d and 3h shows the uniaxial compression tests of the dried GS and GF at different set strains and the recovery abilities for many cycles.

Clearly, for both GS and GF, the curves were non-linear with an increased slope, indicating the elastic buckling of the network. For GS, the curve shows an initial linear region at $\epsilon < 42\%$, and a plateau with gradually increasing slope until very high strains up to 50%, and 93.7% deformation still occurred under 6th loading, indicating a good flexibility. However, for GF, only 54.9% deformation remained under 6th loading (Fig. 3h). It is worth noting that the as-prepared GS showed a high flexibility even at 50% deformation, higher than the value of the porous graphene reported by Xie et al.¹⁸ The reason might be that the large graphene sheets could enhance the integrity of monolith structure.

The Young's Moduli of GS decreased from 7.56 KPa (1st cycle) to 5.98 KPa (6th cycle). But for GF, the value increased from 24.2 KPa to 34.8 KPa, corresponding to severe plastic deformation. It is supposed that the graphene film as a building unit might be responsible for its flexibility in large deformation. The

conductivity of GS (9 mg cm^{-3}) was 54 S m^{-1} , measured by the two-probe method. It should be mentioned that, the resistance of GS increased by only 5% after compress and release for 10 cycles (Fig. S6), showing its potential application in flexible electronics.

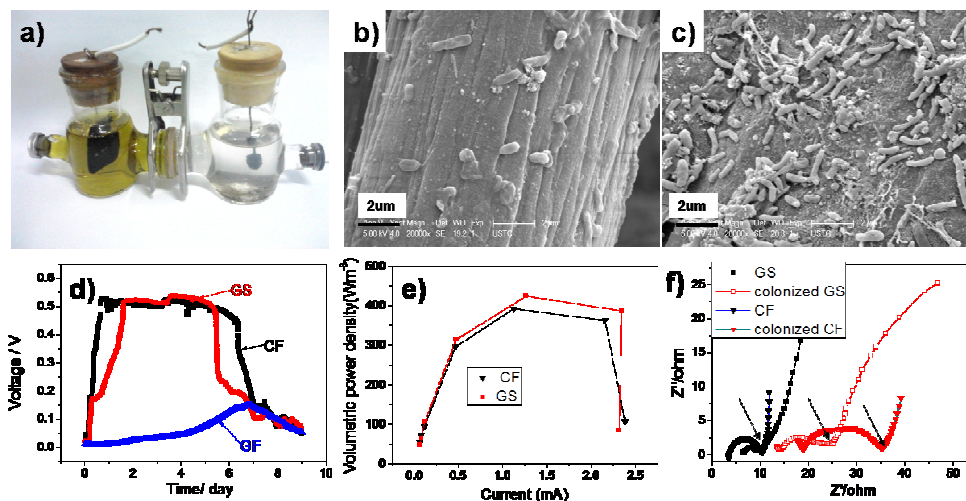


Figure 4. (a) Traditional H-shaped two-chamber MFC equipment; Micrographs of microorganism adhered on carbon fiber (b) and graphene sheet from cross-section of the GS(c); (d) Performance of the H-shaped MFC (HMFC) for different anode materials in batch mode, with 1000Ω external resistor; (e) Polarization curves of HMFCs show the maximum power densities achieved corresponding to GS and CF; (f) Nyquist curves of the electrochemical impedance spectroscopy (EIS) tests for different electrodes before and after colonization. The arrows indicate the point that the system becomes a diffusion control from a kinetic control.

Graphene sponge as the anode in MFC

Carbon materials are potential anode materials for MFC.²¹⁻²⁴ In our previous work,²⁵ it was demonstrated that GO nanoribbons could facilitate the extracellular electron transfer between microbes and electrode. Here, the GS was used as anode in MFC for its good electrical conductivity and macroporous structure, and its open structure facilitated the nutrients transfer for microbes. MFC tests were conducted in conventional H-shaped two-chamber MFC equipment (Fig. 4a), and the electrodes of carbon felt (CF) and GF were employed as control groups. Here, after 2 days of sodium acetate injection, the output voltages of the MFCs with GS and CF exceeded 0.3 V. The MFC performance in the second cycle is shown in Fig. 4d. For both GS and CF their maximum output voltages were in the range of 0.50-0.55 V, while the value of GF was even lower than 0.15 V due to its poor colonization conditions. After one-month operation, the electrodes with microbes were treated by freeze-drying, and the cross-section of electrodes are shown in Fig. 4b and 4c. Clearly, microbes were fixed on both the surface of carbon fiber and graphene sheets from cross-section of GS due to their open structure. On the other hand, no microbes were observed within GF, and biofilm was only formed at the outer surface of GF. In fact, more close to the inner space of GS, the amount of the deposited microbes also decreased, indicating the existence of some closed pore structure or microporous structure where the microbes could not enter (Fig. S8). Therefore, it is still challenge to prepare sponge with overall connected macroporous structure. In addition, much small porous size of GF resulted in bad for the dense porous structure of GF, which is too small for the colonization of bacterial. The power density depends on the current of the cell, and the relationship can be found in Fig.S5

For GS and CF, the maximum power density appeared at 20 h

after the replacement of electrolyte (following the cycle of Fig.4d). The maximum power density generated by GS was 427 Wm^{-3} or 0.71 Wm^{-2} , higher than that of CF at 395 Wm^{-3} or 0.476 Wm^{-2} . (Both power density values were calculated according anode volume and surface.) While the value of GF is only 28 Wm^{-3} . Nyquist curves of the electrochemical impedance spectroscopy (EIS) tests for different electrodes before and after colonization were measured at open circuit potential. It was observed that the interfacial charge transfer resistance of GS was smaller than that of CF both before and after colonization. In addition, GS electrode can support cell for long time for its chemical stability, and the graphene sheets (the blocking units of GS) can facilitate the electron transfer from bacterial to electrode.²⁰ For the large porous structure of GS, the advantages of the high surface to volume ration, and better colonization for bacteria can be utilized, suggesting that GS has potential application as a flexible MFC anode.

Conclusions

Here, a simple but effective method for graphene sponge fabrication is developed. Through controlling the temperature and cooling rate of the ice crystal formation, graphene hydrogel can be assembled into hierarchical macroporous structure. The prepared graphene sponge can recover from 50% deformation repeatedly. As the anode of MFCs, the GS generated the maximum power density of 427 Wm^{-3} , higher than the value of carbon felt at 395 Wm^{-3} . This flexible, conductive, light and highly porous graphene sponge ensures its potential application in MFCs as flexible anode material.

Acknowledgements

This work is supported by the National Basic Research Program of China (No. 2011CB921403 and 2010CB923302), and the National Natural Science Foundation of China (No.51073147).

References

^a Hefei National Laboratory for Physical Sciences at Microscale and Department of Chemical Physics, CAS Key Laboratory of Soft Matter Chemistry, University of Science and Technology of China, Hefei, 230026, P.R. China. Fax: +86-551-63603748; Tel: +86-551-63606853; E-mail: lfyan@ustc.edu.cn

^b Department of Chemistry, University of Science and Technology of China, Hefei, 230026, P.R. China.

[‡] These authors contributed equally.

1. B. E. Logan and K. Rabaey, *Science*, 2012, **337**, 686-690.
2. H. Ren, H.S. Lee, and J. Chae. *Microfluid Nanofluid*, 2012, **13**, 353-381.
3. S. L. Chen, Q. Liu, G. H. He, Y. Zhou, M. Hanif, X. W. Peng, S. Q. Wang and H. Q. Hou, *J. Mater. Chem.*, 2012, **22**, 18609-18613.
4. X. Wang, S. A. Cheng, Y. J. Feng, M. D. Merrill, T. Saito and B. E. Logan, *Environ. Sci. Technol.*, 2009, **43**, 6870-6874.
5. Q. Deng, X. Y. Li, J. E. Zuo, A. Ling and B. E. Logan, *J. Power Sour.*, 2010, **195**, 1130-1135.
6. A. K. Geim, *Science*, 2009, **324**, 1530-1534.
7. S. Park and R. S. Ruoff, *Nat. Nanotechnol.*, 2009, **4**, 217-224.
8. A. A. Balandin, S. Ghosh, W. Z. Bao, I. Calizo, D. Teweldebrhan, F. Miao and C. N. Lau, *Nano Lett.*, 2008, **8**, 902-907.
9. W. F. Chen, S. R. Li, C. H. Chen and L. F. Yan, *Adv. Mater.*, 2011, **23**, 5679-5682.
10. Y. X. Xu, K. X. Sheng, C. Li and G. Q. Shi, *Acs Nano*, 2010, **4**, 4324-4330.
11. W. F. Chen and L. F. Yan, *Nanoscale*, 2011, **3**, 3132-3137.
12. X. C. Dong, H. Xu, X. W. Wang, Y. X. Huang, M. B. Chan-Park, H. Zhang, L. H. Wang, W. Huang and P. Chen, *Acs Nano*, 2012, **6**, 3206-3213.
13. H. C. Bi, X. Xie, K. B. Yin, Y. L. Zhou, S. Wan, L. B. He, F. Xu, F. Banhart, L. T. Sun and R. S. Ruoff, *Adv. Funct. Mater.*, 2012, **22**, 4421-4425.
14. X. Xie, G. Yu, N. Liu, Z. Bao, C. S. Criddle and Y. Cui, *Energy Environ. Sci.*, 2012, **5**, 6862-6866.
15. Y. Z. Zhang, G. Q. Mo, X. W. Li, W. D. Zhang, J. Q. Zhang, J. S. Ye, X. D. Huang and C. Z. Yu, *J. Power Sour.*, 2011, **196**, 5402-5407.
16. H. Wang, G. Wang, Y. Ling, F. Qian, Y. Song, X. Lu, S. Chen, Y. Tong and Y. Li, *Nanoscale*, 2013, **5**, 10283-10290.
17. Z. P. Chen, W. C. Ren, L. B. Gao, B. L. Liu, S. F. Pei and H. M. Cheng, *Nat. Mater.*, 2011, **10**, 424-428.
18. H. F. Zhang, I. Hussain, M. Brust, M. F. Butler, S. P. Rannard and A. I. Cooper, *Nat. Mater.*, 2005, **4**, 787-793.
19. X. Xie, Y. Zhou, H. Bi, K. Yin, S. Wan and L. Sun, *Sci. Rep.*, 2013, **3**.
20. W. F. Chen and L. F. Yan, *Nanoscale*, 2010, **2**, 559-563.
21. S. Nardecchia, D. Carriazo, M. L. Ferrer, M. C. Gutierrez, F. del Monte. *Chem. Soc. Rev.*, 2013, **42**, 794-830.
22. S. Chen, G. He, H. Hu, S. Jin, Y. Zhou, Y. He, F. Zhao, H. Hou. *Energy Environ. Sci.*, 2013, **6**, 2435-2439.
23. T. Zhang, H. Nie, T. S. Bain, H. Lu, M. Cui, O. L. Snoeyenbos-West, A. E. Franks, K. P. Nevin, T. P. Russell, D. R. Lovley. *Energy Environ. Sci.*, 2013, **6**, 217-224.
24. H. Noe, T. Zhang, M. Cui, H. Lu, D. R. Lovley, T. P. Russell. *Phys. Chem. Chem. Phys.*, 2013, **15**, 14290-14294.
25. Y.-X. Huang, X.-W. Liu, J.-F. Xie, G.-P. Sheng, G.-Y. Wang, Y.-Y. Zhang, A.-W. Xu and H.-Q. Yu, *Chem. Commun.*, 2011, **47**, 5795-5797.